Monthly Notices
of the
ROYAL ASTRONOMICAL SOCIETY

MNRAS **505,** 2111–2123 (2021)
Advance Access publication 2021 May 13

https://doi.org/10.1093/mnras/stab1373

Probing modified gravity theories with multiple measurements of high-redshift quasars

Yujie Lian,[1] Shuo Cao,[1]★ Marek Biesiada,[2] Yun Chen,[3] Yilong Zhang[1] and Wuzheng Guo[1]

[1]*Department of Astronomy, Beijing Normal University, Beijing 100875, China*
[2]*National Centre for Nuclear Research, Pasteura 7, PL-02-093 Warsaw, Poland*
[3]*National Astronomical Observatories, Chinese Academy of Sciences, Beijing 100012, China*

Accepted 2021 May 10. Received 2021 April 20; in original form 2021 February 6

ABSTRACT

In this paper, we quantify the ability of multiple measurements of high-redshift quasars to constrain several theories of modified gravity, including the Dvali–Gabadadze–Porrati braneworld scenario, generalized Chaplygin gas, $f(T)$ modified gravity, and modified polytropic Cardassian model. Recently released sample of 1598 quasars with X-ray and ultraviolet flux measurements in the redshift range of $0.036 \leq z \leq 5.1003$, as well as a compilation of 120 intermediate-luminosity radio quasars covering the redshift of $0.46 < z < 2.76$ are respectively used as standard probes at higher redshifts. For all considered modified gravity theories, our results show that there is still some possibility that the standard Λ cold dark matter (ΛCDM) scenario might not be the best cosmological model preferred by the current quasar observations. In order to improve cosmological constraints, the quasar data are also combined with the latest observations of baryon acoustic oscillations, which strongly complement the constraints. Finally, we discuss the support given by the data to modified gravity theories, applying different information theoretic techniques like the Akaike information criterion, Bayesian information criterion, and Jensen–Shannon divergence.

Key words: quasars: general – cosmological parameters – cosmology: observations.

1 INTRODUCTION

The discovery of the accelerating expansion of the Universe, first confirmed by observations of Type Ia supernovae (SNe Ia; Riess et al. 1998; Perlmutter et al. 1999), is a milestone in modern cosmology and has since been verified by other cosmological observations, including the cosmic microwave background (CMB; Spergel et al. 2003), baryon acoustic oscillations (BAO; Eisenstein et al. 2005; Percival et al. 2007), and large-scale structure (Tegmark et al. 2004). However, there are different understandings about the origin of cosmic acceleration, which has led to many cosmological scenarios principally based on two large categories being proposed and developed. On the one hand, in the framework of Einstein's theory of general relativity a mysterious component with negative pressure, dubbed dark energy (DE; Copeland, Sami & Tsujikawa 2006), responsible for the accelerated cosmological expansion is proposed. On the other hand, modifying the theory of gravity (Tsujikawa 2010) is another direction to understand this phenomenon instead of adding new hypothetical material components.

In the first scenario, the simplest candidate for DE is the cosmological constant Λ, a modification of the energy–momentum tensor in Einstein equations, which is constant in time and underlies the simplest standard cosmological model – the Λ cold dark matter (ΛCDM) model. While ΛCDM is consistent with many observations (Allen et al. 2008; Cao et al. 2012a; Alam et al. 2017; Farooq et al. 2017; Scolnic et al. 2018), this model is still confronted with some theoretical problems such as the well-known fine-tuning problem and coincidence problem (Weinberg 1989), which has prompted a great number of DE models including dynamic DE models (Boisseau et al. 2000; Kamenshchik, Moschella & Pasquier 2001; Maor, Brustein & Steinhardt 2001), interacting DE model (Amendola 2000; Caldera-Cabral, Maartens & Urena-Lopez 2009), and scalar field theories (Peebles & Ratra 1988; Ratra & Peebles 1988; Zlatev, Wang & Steinhardt 1999; Caldwell & Linder 2005; Chen & Ratra 2011; Chen et al. 2016) to be proposed and studied. In the second scenario, many modified gravity theories not only provide interesting ideas to deal with the cosmological constant problem and explain the late-time acceleration of the Universe without DE, but also describe the large-scale structure distribution of the Universe (see Clifton et al. 2012; Koyama 2016 for recent reviews). One idea to modify gravity is assuming that our universe is embedded in a higher dimensional space–time, such as the braneworld Dvali–Gabadadze–Porrati (DGP) model (Dvali, Gabadadze & Porrati 2000; Sollerman et al. 2009), modified polytropic Cardassian (MPC) model (Wang et al. 2003; Magana et al. 2015), and Gauss–Bonnet gravity (Nojiri & Odintsov 2005). Another interesting idea is to extend general relativity (GR) by permitting the field equation to be higher than second order, like $f(R)$ gravity (Chiba 2003; Sotiriou & Faraoni 2010), or change the Levi–Civita connection to the Weitzenböck connection with torsion, such as $f(T)$ gravity (Bengochea et al. 2009; Yang 2011; Cai et al. 2016). In this paper, we concentrate on four cosmological models in the framework work of Friedman–Lemaître–Robertson–Walker metric, including generalized Chaplygin gas (GCG) model, a kind of dynamical DE model, in which the DE density decreases with time, DGP model, MPC model, and the power-law $f(T)$ model, based on teleparallel gravity.

With so many competitive cosmological models, many authors have taken advantage of various cosmological probes, such as SN Ia

★ E-mail: caoshuo@bnu.edu.cn

(Nesseris et al. 2005; Suzuki et al. 2012; Scolnic et al. 2018), gamma-ray burst (Lamb & Reichart 2000; Liang & Zhang 2005; Ghirlanda, Ghisellini & Firmani 2006; Rezaei, Ojaghi & Malekjani 2020), H II starburst galaxies (Siegel et al. 2005; Plionis et al. 2011; Terlevich et al. 2015; Wei, Wu & Melia 2016; Cao, Ryan & Ratra 2020b; Wu et al. 2020) acting as standard candles, strong gravitational lensing systems (Biesiada, Malec & Piorkowska 2011; Cao, Zhu & Zhao 2011; Cao & Zhu 2012; Cao, Covone & Zhu 2012b; Cao et al. 2012a, 2015, 2017c; Chen et al. 2015; Liu et al. 2019a; Amante et al. 2020), galaxy clusters (Bonamente et al. 2006; De Bernardis, Giusarma & Melchiorri 2006; Chen & Ratra 2012), BAO measurements, CMB (Spergel et al. 2003; Planck Collaboration XIII 2016; Planck Collaboration VI 2020) acting as standard rulers to test these models or in other similar cosmological studies. Furthermore, it is crucial to test which model is most favoured by current observations, in addition to the most important aim that is to constrain cosmological parameters more precisely. To fulfil this tough goal, better and diverse data sets are required.

Recently, quasars observed with multiple measurements, another potential cosmological probe with a higher redshift range that reaches to $z \sim 5$, is becoming popular to constrain cosmological models in the largely unexplored portion of redshift range from $z \sim 2$ to $z \sim 5$. A sample that contains 120 angular size measurements in intermediate-luminosity quasars from the very long baseline interferometry (VLBI) observations (Cao et al. 2017a,b) has become an effective standard ruler, which have been extensively applied to test cosmological models (Li et al. 2017; Melia et al. 2017; Qi et al. 2017; Zheng et al. 2017; Xu et al. 2018; Ryan, Chen & Ratra 2019), measuring the speed of light (Cao et al. 2017a, 2020a), exploring cosmic curvature at different redshifts (Cao et al. 2019; Qi et al. 2019), and the validity of cosmic distance duality relation (Zheng et al. 2020). Then, Risaliti & Lusso (2019) put forward a new compilation of quasars containing 1598 quasi-stellar object (QSO) X-ray and ultraviolet (UV) flux measurements in the redshift range of $0.036 \leq z \leq 5.1003$, which have been used to constrain cosmological models (Khadka & Ratra 2020b) and cosmic curvature at high redshifts (Liu et al. 2020a,c), as well as test the cosmic opacity (Geng et al. 2020; Liu et al. 2020b). Making use of this data to explore cosmological researches mainly depends on the empirical relationship between the X-ray and UV luminosity of these high-redshift quasars proposed by Avni & Tananbaum (1986), which leads to the Hubble diagram constructed by quasars (Risaliti & Lusso 2015, 2017; Lusso & Risaliti 2016; Bisogni, Risaliti & Lusso 2017). In general, the advantage of these two QSO measurements over other traditional cosmological probes is that QSO has a larger redshift range, which may be rewarding in exploring the behaviour of the non-standard cosmological models at high redshifts, providing an important supplement to other astrophysical observations and also demonstrating the ability of QSO as an additional cosmological probe (Zheng et al. 2021).

In this paper, we focus on applying the angular size measurements of intermediate-luminosity quasars (Cao et al. 2017a,b) and the large QSO X-ray and UV flux measurements (Risaliti & Lusso 2019) to constrain four non-standard cosmological models, with the main goal of testing the agreement between the high-redshift combined QSO data and the standard ΛCDM model through the performance of these non-standard models at higher redshift, as well as demonstrating the potential of QSO as an additional cosmological probe. In order to make the constraints more stringent and test consistency, 11 recent BAO measurements (Cao et al. 2020b) are considered in the joint analysis with the combined QSO measurements, at the redshift range $0.122 \leq z \leq 2.34$. This paper is organized as follows. In Section 2, all the observations we used in this work are briefly introduced. In Section 3, we describe the non-standard cosmological models we considered, and details of the methods used to constrain the model parameters are described in Section 4. In Section 5, we perform a Markov chain Monte Carlo (MCMC) analysis using different data sets, and apply some techniques of model selection. Finally, conclusions are summarized in Section 6.

2 DATA

Quasars are one of the brightest sources in the Universe. Observable at very high redshifts, they are regarded as particularly promising cosmological probes. In the past decades, different relations involving the quasar luminosity have been proposed to study the 'redshift–luminosity distance' relation in quasars with the aim of cosmological applications (Baldwin 1977; Watson et al. 2011; Wang et al. 2013). Accordingly, Risaliti & Lusso (2015) compiled a sample of 808 quasar flux–redshift measurements over a redshift range $0.061 \leq z \leq 6.280$ with the aim to constrain cosmological models. More than three-quarters of quasars in this sample are located at high redshift ($z > 1$). It is worth to notice that this compilation alone did not give very tight constraints on the cosmological parameters compared with other data (Khadka & Ratra 2020a), on account of the large global intrinsic dispersion ($\delta = 0.32$) in the X-ray and UV luminosity relation. Recently, Risaliti & Lusso (2019) proposed a final compilation of 1598 quasars flux–redshift measurements, selected from a sample of 7238 quasars with available X-ray and UV measurements, to find more high-quality quasars applicable to cosmological research. Compared with the 2015 data set, the latest quasar sample has a smaller redshift range ($0.036 \leq z \leq 5.1003$), whereas 899 quasars at high redshift ($z > 1$) are included in the sample. Meanwhile, with the progressively refined selection technique, flux measurements, and the efforts of eliminating systematic errors, the Hubble diagram produced by this large quasar sample is in great accordance with that of supernovae and the concordance model at $z \leq 1.4$ (Risaliti & Lusso 2019). Besides, these QSOs have an X-ray and UV luminosity relation with a smaller intrinsic dispersion ($\delta = 0.23$).

Besides the X-ray and UV flux measurements of quasars, we also use the angular size measurements in radio quasars (Cao et al. 2017a,b, 2018), from the VLBI observations, which has become a reliable standard ruler in cosmology. The measurements of milliarcsecond-scale angular size from compact radio sources (Gurvits, Kellermann & Frey 1999) have been utilized for cosmological models inference (Vishwakarma 2001; Zhu & Fujimoto 2002; Chen & Ratra 2003). Notably, the angular size measurements are effective only if the linear size $l_{\rm m}$ of the compact radio sources is independent on both redshifts and intrinsic properties of the source such as luminosity. More recently, Cao et al. (2017b) presented a final sample of 120 intermediate-luminosity quasars ($10^{27} \leq L \leq 10^{28}$ W Hz^{-1}) over the redshift range $0.46 < z < 2.76$ from VLBI all-sky survey of 613 milliarcsecond ultracompact radio sources (Kellermann 1993; Gurvits 1994), in which these intermediate-luminosity quasars show negligible dependence on redshifts and intrinsic luminosity. Meanwhile, a cosmology-independent method to calibrate the linear size as $l_{\rm m} = 11.03$ pc was implemented in the study and these angular size versus redshift data have been used to constrain cosmological parameters.

Additionally, in order to acquire smaller uncertainty, as well as to compare the constraints to the joint analysis with other cosmological probes, we also add 11 recent BAO data (Cao et al. 2020b) in our analysis. These data come from the large-scale structure power spectrum through astronomical surveys and have been extensively

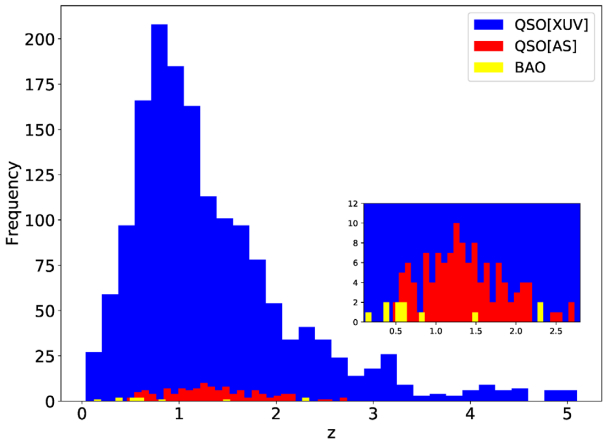

Figure 1. The redshift distribution of the QSO and BAO measurements and its details (lower right). Blue, red, and yellow histograms stand for the redshift distribution of QSO[XUV], QSO[AS], and BAO, respectively.

applied in cosmological applications, covering the redshift range $0.122 \leq z \leq 2.34$. Fig. 1 indicates the redshift distribution of the QSO measurements and BAO data, where we display the X-ray and UV fluxes QSO measurements, the angular size measurements in radio quasars, and BAO measurements by the abbreviation QSO[XUV], QSO[AS], and BAO, respectively.

3 COSMOLOGICAL MODELS

In this paper, we concentrate on four non-standard cosmological models in a spatially flat universe, including the DGP model, GCG model, the MPC model, and the power-law $f(T)$ model, based on teleparallel gravity.

3.1 Dvali–Gabadadze–Porrati model

Arising from the braneworld theory, the Dvali–Gabadadze–Porrati (DGP) model (Dvali et al. 2000) modifies the gravity to reproduce the cosmic acceleration without need to invoke DE. In this model, we are living on a 4D membrane in a higher dimensional space–time. Moreover, the gravity leaks out into the bulk at large scales, which will result in the accelerated expansion of the Universe (Li et al. 2013). The Friedman equation is modified as

$$H^2 - \frac{H}{r_c} = \frac{8\pi G}{3}\rho_m, \tag{1}$$

where $r_c = 1/[H_0(1-\Omega_m)]$ represents the length scale beyond which the leaking occurs. We can directly rewrite the above equation and get the expansion rate

$$\frac{H(z)^2}{H_0^2} = \left(\sqrt{\Omega_m(1+z)^3 + \Omega_{rc}} + \sqrt{\Omega_{rc}}\right)^2, \tag{2}$$

where H_0 is the Hubble constant and $\Omega_{rc} = 1/(4r_c^2H_0^2)$ is related to the cosmological scale. Setting $z = 0$ in equation (2), the normalization condition can be obtained

$$\Omega_{rc} = \frac{(1-\Omega_m)^2}{4}, \tag{3}$$

and there are two free parameters $\hat{p} = (\Omega_m, H_0)$ to be constrained.

3.2 Generalized Chaplygin gas model

As one of the candidates for DE models, the Chaplygin gas model, where DE and dark matter are unified through an exotic equation of state, has been proposed to explain the cosmic acceleration (Kamenshchik et al. 2001; Bento, Bertolami & Sen 2002; Biesiada, Godłowski & Szydłowski 2005; Malekjani, Khodam-Mohammadi & Nazari-pooya 2011). In this model, the Universe is filled with the so-called Chaplygin gas, which is a perfect fluid characterized by the equation of state $p = -A/\rho$. A more general case, in which

$$p = -\frac{A}{\rho^\alpha}, \tag{4}$$

where A is a positive constant and ρ is the energy density of this fluid, is called the generalized Chaplygin gas (GCE). The GCG model with $\alpha = 0$ reduces to standard ΛCDM model and with $\alpha = 1$ reduces to the standard Chaplygin gas (SCG) model. In the framework of Friedmann–Lemaître–Robertson–Walker (FLRW) metric, applying equation (4) and the conservation equation $\mathrm{d}(\rho a^3) = -p\mathrm{d}(a^3)$, the energy density of GCG model is written as

$$\rho_{GCG} = \rho_{0GCG}\left[A_s + (1-A_s)a^{-3(1+\alpha)}\right]^{\frac{1}{1+\alpha}}, \tag{5}$$

where a is the scale factor, $A_s = A/\rho_{0GCG}^{1+\alpha}$, and ρ_{0GCG} is the present energy density of the GCG. Using equations (4) and (5), one obtains the equation-of-state parameter of GCG model,

$$\omega_{GCG} = -\frac{A_s a^{3(1+\alpha)}}{1 - A_s + A_s a^{3(1+\alpha)}}. \tag{6}$$

Equation (6) shows clearly that GCG acts like dust matter ($\omega_{GCG} \to 0$) in the early time ($a \to 0$) and behaves like a cosmological constant ($\omega_{GCG} \to -1$) at late epoch ($a \to \infty$). The Friedman equation for this model can be expressed as

$$H(z)^2/H_0^2 = \Omega_b(1+z)^3 + (1-\Omega_b)\left[A_s + (1-A_s)(1+z)^{3(1+\alpha)}\right]^{\frac{1}{1+\alpha}}, \tag{7}$$

where Ω_b is the present density parameter of the baryonic matter. We adopt $100\Omega_b h^2 = 2.166 \pm 0.015 \pm 0.011$ with $h = H_0/100$ as usual and in the uncertainty budget first term is associated with the deuterium abundance measurement and the second one – with the big bang nucleosynthesis (BBN) calculation – used to get Ω_{b0} (Cooke, Pettini & Steidel 2018). Since the parameter A_s can be expressed by the effective total matter density Ω_m and the α parameter,

$$A_s = 1 - \left(\frac{\Omega_m - \Omega_b}{1-\Omega_b}\right)^{1+\alpha}, \tag{8}$$

there are three free parameters $\hat{p} = (\Omega_m, \alpha, H_0)$ in this model.

3.3 Power-law $f(T)$ model

Lately, another kind of modified gravity theory, $f(T)$ (Bengochea et al. 2009; Cai et al. 2016; Qi et al. 2017), proposed in the framework of the teleparallel equivalent of GR, has attracted a lot of attention. In this scenario, the Weitzenböck connection with torsion is used instead of torsionless Levi–Civita connection with curvature used in GR. The Lagrangian density is a function $f(T)$ of the torsion scalar T, which is responsible for the cosmic acceleration. In this framework, the Friedman equation could be expressed as

$$\frac{H(z)^2}{H_0^2} = \Omega_m(1+z)^3 + \Omega_F y(z, P), \tag{9}$$

where $\Omega_F = 1 - \Omega_m$ and $y(z, \hat{p})$ can be written as

$$y(z, \hat{p}) = \frac{1}{T_0 \Omega_F}(f - 2T f_T), \tag{10}$$

with $T_0 = -6H_0^2$, $f_T \equiv df/dT$, and $\hat{p}$ representing the parameters occurring in different forms of $f(T)$ theory. In this paper, we focus on the power-law $f(T)$ model with the following form:

$$f(T) = \alpha(-T)^b, \tag{11}$$

where α and b are two model parameters. The distortion parameter b quantifies the deviation from the ΛCDM model, while the parameter α can be expressed through the Hubble constant and density parameter Ω_{F0} by combining equations (9) and (11) with the boundary condition $H(z = 0)/H_0 = 1$:

$$\alpha = (6H_0^2)^{1-b}\frac{\Omega_{F0}}{2b - 1}. \tag{12}$$

Now, equation (10) can be rewritten as

$$y(z, \hat{p}) = E^{2b}(z, b). \tag{13}$$

Here we consider the Taylor expansion up to second order for equation (9), on $H(z, b)^2/H_0^2$ around $b = 0$, to calculate the Friedman equation (details can be found in Nesseris et al. 2013). Eventually, the free parameters in this $f(T)$ model are $\hat{p} = (\Omega_m, b, H_0)$.

3.4 Modified polytropic Cardassian model

In order to explain the accelerated cosmological expansion from a different perspective, Freese & Lewis (2002) introduced the original Cardassian model motivated by the braneworld theory, without DE involved. In this model the Friedman equation is modified to

$$H^2 = \frac{8\pi G\rho_m}{3} + B\rho_m^n, \tag{14}$$

where ρ_m is the total matter density and the second term on the right-hand side represents the Cardassian term. It is worth noting that the Universe is driven to accelerate by the Cardassian term when the parameter n satisfies $n < 2/3$. Then, a simple generalized case of the Cardassian model was proposed by Gondolo & Freese (2002) and Wang et al. (2003), where an additional exponent q was introduced. We can write the Friedman equation with this generalization as

$$\frac{H(z)^2}{H_0^2} = \Omega_m(1+z)^3\left[1 + \left(\left(\frac{1}{\Omega_m}\right)^q - 1\right)(1+z)^{3q(n-1)}\right]^{1/q}. \tag{15}$$

The MPC model, with the free parameters of $\hat{p} = (\Omega_m, n, q, H_0)$ in this model, will reduce to ΛCDM model when $q = 1$ and $n = 0$.

4 METHODS

In this section, we present the details of deriving observational constraints on the cosmological models from QSOs and BAO measurements.

4.1 Quasars measurements

Over the decades, a non-linear relation between the UV and X-ray luminosities of quasars has been recognized and refined (Risaliti & Lusso 2015). This relation can be expressed as

$$\log(L_X) = \gamma\log(L_{UV}) + \beta, \tag{16}$$

where $\log = \log_{10}$ and the slope – γ along with the intercept – β are two free parameters, which should be constrained by the measurements. Applying the flux–luminosity relation of $F = L/4\pi D_L^2$, the UV and X-ray luminosities can be replaced by the observed fluxes:

$$\log(F_X) = \gamma\log(F_{UV}) + 2(\gamma - 1)\log(D_L) + (\gamma - 1)\log(4\pi) + \beta, \tag{17}$$

where F_X and F_{UV} are the X-ray and UV fluxes, respectively. Here D_L is the luminosity distance, which indicates such kind of QSO measurements can be used to calibrate them as standard candles. Theoretically, D_L is determined by the redshift z and cosmological parameters $\hat{p}$ in a specific model:

$$D_L(z, \hat{p}) = \frac{c(1+z)}{H_0}\int_0^z \frac{dz'}{E(z')}, \tag{18}$$

where $E(z) \equiv H(z)/H_0$. In order to constrain cosmological parameters $\hat{p}$ through the measurements of QSO X-ray and UV fluxes, we compare the observed X-ray fluxes with the predicted X-ray fluxes calculated with equation (17) at the same redshift. Then, the best-fitting parameter values and respective uncertainties for each cosmological model are determined by minimizing the $\chi^2 = -2\ln(\mathrm{LF})$ objective function, defined by the log-likelihood (Risaliti & Lusso 2015):

$$\ln(\mathrm{LF}) = -\frac{1}{2}\sum_{i=1}^{1598}\left[\frac{\left[\log\left(F_{X,i}^{obs}\right) - \log\left(F_{X,i}^{th}\right)\right]^2}{s_i^2} + \ln\left(2\pi s_i^2\right)\right], \tag{19}$$

where $\ln = \log_e$, $s_i^2 = \sigma_i^2 + \delta^2$, and $\ln\sigma_i$ is the measurement error on $F_{X,i}^{obs}$. In addition to the cosmological model parameters, three more free parameters are fitted: γ, β representing the X–UV relation, and δ representing the global intrinsic dispersion. Then, according to Khadka & Ratra (2020b), for the purpose of model comparison we use the value of

$$\chi^2_{XUV,min} = -2\ln(\mathrm{LF})_{min} - \sum_{i=1}^{1598}\ln\left(2\pi\left(\sigma_{i,XUV}^2 + \delta_{best\ fit}^2\right)\right). \tag{20}$$

In our analysis, another QSO data set comes from a new compiled sample of 120 intermediate-luminosity quasars (Cao et al. 2017a,b) covering the redshift range $0.46 < z < 2.76$ with angular sizes $\theta_{obs}(z)$, while the intrinsic length of this standard ruler is calibrated to $l_m = 11.03 \pm 0.25$ pc through a new cosmology-independent calibration technique (Cao et al. 2017b). The corresponding theoretical predictions for the angular sizes at redshift z can be expressed as

$$\theta_{th}(z) = \frac{l_m}{D_A(z)}, \tag{21}$$

where $D_A(z)$ is the angular diameter distance at redshift z and

$$D_A(z) = \frac{D_L(z)}{(1+z)^2}. \tag{22}$$

Then, one can derive model parameters by minimizing the χ^2 objective function:

$$\chi^2_{AS}(z; \hat{p}) = \sum_{i=1}^{120}\frac{[\theta_{th}(z_i; \hat{p}) - \theta_{obs}(z_i)]^2}{\sigma_\theta(z_i)^2}, \tag{23}$$

where $\hat{p}$ denote free parameters in a specific cosmological model and $\theta_{th}(z_i; \hat{p})$ represents the theoretical value of angular sizes at redshift z_i. Moreover, an additional 10 per cent systematical uncertainty is added in the total uncertainty $\sigma_\theta(z_i)^2$ to account for the intrinsic spread in the linear size (Cao et al. 2017b). Therefore, in our analysis, the total uncertainty is written as $\sigma_\theta(z_i)^2 = \sigma_{\theta,\,stat}(z_i)^2 +$

Table 1. The BAO data. Distances $D_M(r_{s,\,fid}/r_s)$, $D_V(r_{s,\,fid}/r_s)$, r_s, and $r_{s,\,fid}$ have the units of Mpc, $H(z)(r_s/r_{s,\,fid})$ has the units of km s^{-1} Mpc^{-1}, and D_A/r_s, D_H/r_s, and D_M/r_s are dimensionless.

z	Measurement	Value	Ref.
0.38	$D_M(r_{s,\,fid}/r_s)$	1512.39	Alam et al. (2017)
0.38	$H(z)(r_s/r_{s,\,fid})$	81.2087	Alam et al. (2017)
0.51	$D_M(r_{s,\,fid}/r_s)$	1975.22	Alam et al. (2017)
0.51	$H(z)(r_s/r_{s,\,fid})$	90.9029	Alam et al. (2017)
0.61	$D_M(r_{s,\,fid}/r_s)$	2306.68	Alam et al. (2017)
0.61	$H(z)(r_s/r_{s,\,fid})$	98.9647	Alam et al. (2017)
0.122	$D_V(r_{s,\,fid}/r_s)$	539 ± 17	Carter et al. (2018)
0.81	D_A/r_s	10.75 ± 0.43	Abbott et al. (2019b)
1.52	$D_V(r_{s,\,fid}/r_s)$	3843 ± 147	Ata et al. (2018)
2.34	D_H/r_s	8.86	de Sainte Agathe et al. (2019)
2.34	D_M/r_s	37.41	de Sainte Agathe et al. (2019)

Note. The correlation matrix of the six measurements from Alam et al. (2017) and the two measurements from de Sainte Agathe et al. (2019) can be found in Ryan et al. (2019) and Cao et al. (2020b), respectively.

$\sigma_{\theta,\,sys}(z_i)^2$, where $\sigma_{\theta,\,stat}(z_i)^2$ is the statistical uncertainty of $\theta_{obs}(z_i)$ measurements.

4.2 Baryon acoustic oscillations measurements

For inclusion of the baryon acoustic oscillations (BAO) measurements to the determination of cosmological parameters, we follow the approach carried out in Ryan et al. (2019). It is well known that the BAO data, in particular those listed in Table 1, are scaled by the size of the sound horizon at the drag epoch r_s, which can be expressed as (details can be found in Eisenstein & Hu 1998)

$$r_s = \frac{2}{3k_{eq}}\sqrt{\frac{6}{R_{eq}}}\ln\left[\frac{\sqrt{1+R_d}+\sqrt{R_d+R_{eq}}}{1+\sqrt{R_{eq}}}\right], \tag{24}$$

where R_d and R_{eq} are the values of the baryon to photon density ratio,

$$R = \frac{3\rho_b}{4\rho_\gamma}, \tag{25}$$

at the drag and matter-radiation equality redshifts z_d and z_{eq}, respectively, and k_{eq} is the particle horizon wavenumber at z_{eq}. The detailed expression of z_d, z_{eq}, k_{eq}, and the baryon to photon density radio R can be found in Eisenstein & Hu (1998).

The BAO measurements listed in Table 1 involve the transverse comoving distance (equal to the line-of-sight comoving distance if $\Omega_{k0} = 0$),

$$D_M(z) = D_c(z) = \frac{c}{H_0}\int_0^z \frac{dz'}{E(z')}, \tag{26}$$

the expansion rate $H(z)$, angular diameter distance $D_A(z) = \frac{D_M(z)}{1+z}$, and the volume-averaged angular diameter distance,

$$D_V(z) = \left[\frac{cz}{H_0}\frac{D_M^2(z)}{E(z)}\right]^{1/3}. \tag{27}$$

For the measurements of the sound horizon (r_s) scaled by its fiducial value, we use equation (24) to calculate both r_s and $r_{s,\,fid}$, following the approach applied in Ryan et al. (2019). The parameters of (Ω_m, H_0, $\Omega_b h^2$) in the fiducial cosmology are used as input to compute $r_{s,\,fid}$ where the BAO measurements are reported. For the analysis that scales the BAO measurements only by r_s, we turn to the fitting formula of Eisenstein & Hu (1998), which is modified with a multiplicative scaling factor of 147.60 Mpc/$r_{s,\,Planck}$. According to the analysis of Ryan et al. (2019), such modifications to the output of the fitting formula may result in precise determinations of the size of the sound horizon r_s and $r_{s,\,fid}$. Let us note that the baryon density $\Omega_b h^2$ is required to calculate the sound horizon r_s in equation (24). For the uncorrelated BAO measurements listed in Table 1 (i.e. rows 7–9), the χ^2 objective function can be written as

$$\chi^2_{BAO}(\hat{p}) = \sum_{i=1}^{3}\frac{[A_{th}(z_i;\hat{p}) - A_{obs}(z_i)]^2}{\sigma(z_i)^2}, \tag{28}$$

where A_{th} and A_{obs} are the predicted and measured quantities of the BAO data listed in Table 1, and $\sigma(z_i)$ stands for the relevant uncertainty of A_{obs}.

The BAO measurements listed in the first six rows and the last two rows of Table 1 are correlated and consequently the χ^2 objective function takes the form

$$\chi^2_{BAO}(\hat{p}) = [A_{th}(\hat{p}) - A_{obs}]^T\,\mathbf{C}^{-1}\,[A_{th}(\hat{p}) - A_{obs}], \tag{29}$$

where $\mathbf{C}^{-1}$ denotes the inverse covariance matrix (Ryan et al. 2019) for the BAO data taken from Alam et al. (2017), while the covariance matrix is presented in Cao et al. (2020b) for the BAO data taken from de Sainte Agathe et al. (2019).

4.3 Joint analysis

We will perform the joint analysis of the above described data to determine constraints on the parameters of a given model. In this section we outline the underlying methodology. Using the χ^2objective function defined above, one can write the likelihood function as

$$\mathcal{L}(\hat{p}) = e^{-\frac{\chi(\hat{p})^2}{2}}, \tag{30}$$

where $\hat{p}$ is the set of model parameters under consideration. Then, the likelihood function of the above combined analysis is expressed as

$$\mathcal{L} = \mathcal{L}_{XUV}\mathcal{L}_{AS}\mathcal{L}_{BAO}. \tag{31}$$

The likelihood analysis is performed using the MCMC method, implemented in the emcee package[1] in python 3.7 (Foreman-Mackey et al. 2013).

After constraining the parameters of each model, it is essential to determine which model is most preferred by the observational measurements and carry out a good comparison between the different models. Out of possible model selection techniques, we will use the Akaike information criterion (AIC; Akaike 1974),

$$AIC = \chi^2_{min} + 2k, \tag{32}$$

and the Bayesian information criterion (BIC; Schwarz 1978),

$$BIC = \chi^2_{min} + k\ln N, \tag{33}$$

where $\chi^2_{min} = -2\ln\mathcal{L}_{max}$, k is the number of free parameters in the model, and N represents the number of data points. Moreover, the ratio of χ_{min} to the number of degrees of freedom (dof) $= N - k$ is reported as an estimate of the quality of the observational data set. The Akaike weights ω_i(AIC) and Bayesian weights ω_i(BIC) are computed through the normalized relative model likelihoods, which are expressed as

$$\omega_i(IC) = \frac{\exp\left\{-\frac{1}{2}\Delta_i(IC)\right\}}{\sum_{k=1}^{K}\exp\left\{-\frac{1}{2}\Delta_k(IC)\right\}}, \tag{34}$$

[1] https://pypi.python.org/pypi/emcee

where Δ_i(IC) is the difference of the value of given information criterion IC (AIC or BIC) between the model i and the one which has the lowest IC, and K denotes the total number of the models considered. One can find the details of the rules for estimating the AIC and BIC model selection in Biesiada (2007) and Lu et al. (2008).

We supplement the model comparison by calculating the Jensen–Shannon divergence (JSD; Lin 1991; Abbott et al. 2019a) between the posterior distributions of the common parameters assessed with two different cosmological models. The JSD is a symmetrized and smoothed measure of the distance between two probability distributions $p(x)$ and $q(x)$ defined as

$$D_{\rm JS}(p \mid q) = \frac{1}{2}\left[D_{\rm KL}(p \mid s) + D_{\rm KL}(q \mid s)\right], \tag{35}$$

where $s = 1/2(p + q)$ and $D_{\rm KL}$ is the Kullback–Leibler divergence (KLD) between the distributions $p(x)$ and $q(x)$ expressed as

$$D_{\rm KL}(p \mid q) = \int p(x) \log_2 \left(\frac{p(x)}{q(x)}\right) {\rm d}x, \tag{36}$$

and a smaller value of the JSD indicates that the posteriors from two models agree well (Abbott et al. 2019a).

It should be pointed out that in order to compare models through the JSD, we should use the posterior distributions of parameters $\hat{p}$ that are the same in the models compared. Therefore, the matter density $\Omega_{\rm m}$ and the Hubble constant H_0 are the two parameters of interest in our analysis. In addition, we will compare the models described in Section 3 with ΛCDM model. Concerning the posterior distributions of common free parameters in different models, they can be obtained through the MCMC method, then we take advantage of the dedicated PYTHON 3.7 package[2] (Virtanen et al. 2020) to compute the JSD between two one-dimensional (1D) probability distributions.

5 RESULTS AND DISCUSSION

In this section, we present the results for the four cosmological models listed in Section 3, obtained using different combination of data sets: QSO[XUV]+QSO[AS], BAO, and QSO[XUV]+QSO[AS]+BAO. In order to have a good comparison, the corresponding results for the concordance ΛCDM model is also displayed. The 1D probability distributions and two-dimensional (2D) contours with 1σ and 2σ confidence levels, and the best-fitting value with 1σ uncertainty for each model are shown in Figs 2–6 and reported in Table 2.

5.1 Observational constraints on Dvali–Gabadadze–Porrati model

As can be seen from Fig. 3, the combined QSO measurements (QSO[XUV]+QSO[AS]) do not provide stringent constraints on the matter density parameter $\Omega_{\rm m}$, which will be improved with the combination of recent BAO observations. The best-fitting value of $\Omega_{\rm m}$ given by QSO[XUV]+QSO[AS] is $\Omega_{\rm m} = 0.365^{+0.129}_{-0.100}$ within 68.3 per cent confidence level, which agrees well with the QSO[AS] data alone: $\Omega_{\rm m} = 0.285^{+0.255}_{-0.155}$ (without systematics; Cao et al. 2017b), the recent *Planck* 2018 results: $\Omega_{\rm m} = 0.315 \pm 0.007$ (Planck Collaboration VI 2020), and SNe Ia+BAO+CMB+observational Hubble parameter (OHD): $\Omega_{\rm m} = 0.305 \pm 0.015$ (Shi, Huang & Lu 2012). However, it is worthwhile to mention that the matter density parameter $\Omega_{\rm m}$ obtained by QSO tends to be higher

[2]scipy.spatial.distance.jensenshannon

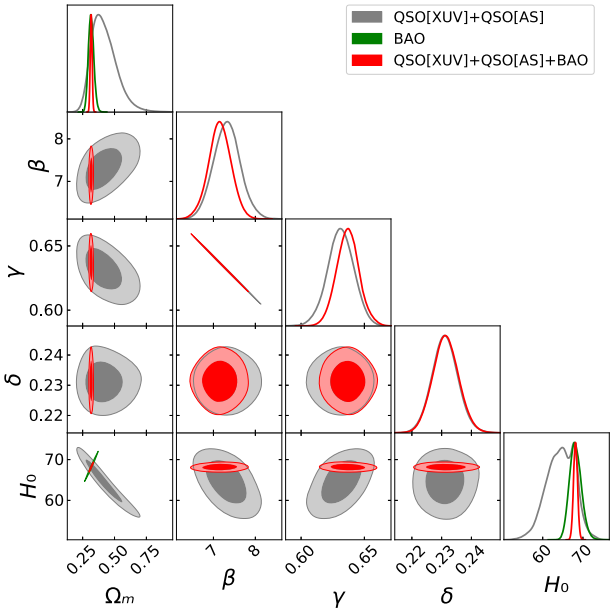

Figure 2. The 1D probability distributions and 2D contours with 1σ and 2σ confidence levels for ΛCDM model obtained from QSO[XUV]+QSO[AS] (grey), BAO (green), and QSO[XUV]+QSO[AS]+BAO (red) data.

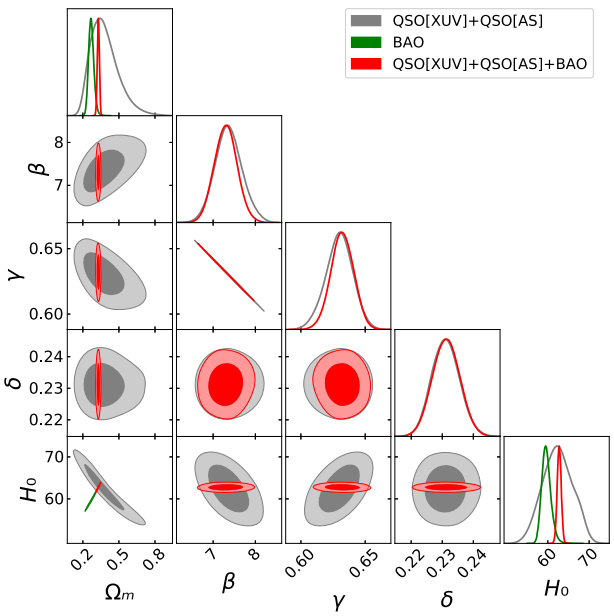

Figure 3. The 1D probability distributions and 2D contours with 1σ and 2σ confidence levels for DGP model obtained from QSO[XUV]+QSO[AS] (grey), BAO (green), and QSO[XUV]+QSO[AS]+BAO (red) data.

than that from other cosmological probes, as was remarked in the previous works of Risaliti & Lusso (2019) and Khadka & Ratra (2020b). This suggests that the composition of the Universe characterized by cosmological parameters can be comprehended differently through high-redshift quasars. For the BAO data, the best-fitting matter density parameter is $\Omega_{\rm m} = 0.269^{+0.022}_{-0.020}$, which is significantly lower than that from the modified gravity theories considered in this paper. Interestingly, the estimated values of $\Omega_{\rm m}$ are in agreement with the standard ones reported by other astrophysical probes, such as $\Omega_{\rm m} = 0.277^{+0.017}_{-0.017}$ given by the linear

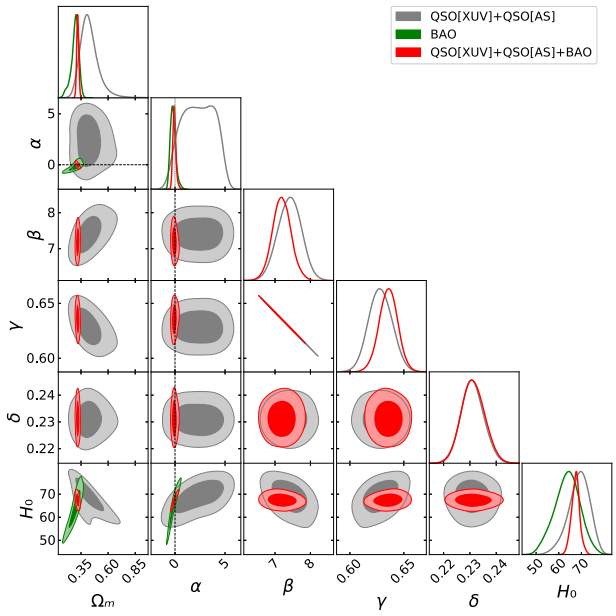

Figure 4. The 1D probability distributions and 2D contours with 1σ and 2σ confidence levels for GCG model obtained from QSO[XUV]+QSO[AS] (grey), BAO (green), and QSO[XUV]+QSO[AS]+BAO (red) data. The black dashed line represents the ΛCDM model corresponding to $\alpha = 0$.

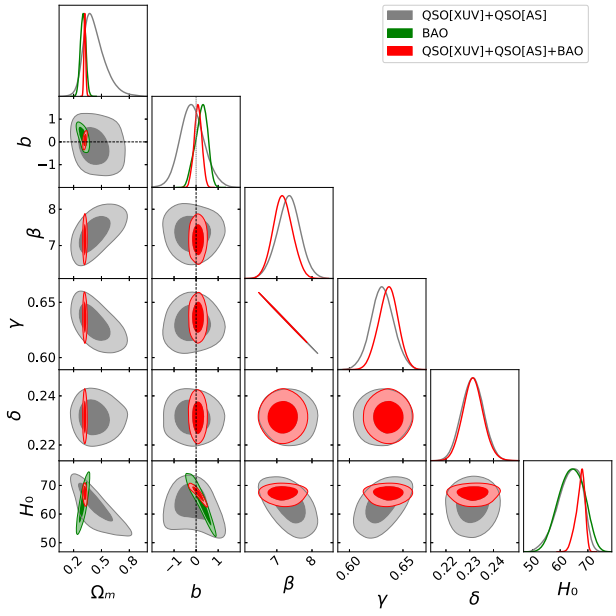

Figure 5. The 1D probability distributions and 2D contours with 1σ and 2σ confidence levels for $f(T)$ model obtained from QSO[XUV]+QSO[AS] (grey), BAO (green) and QSO[XUV]+QSO[AS]+BAO (red) data. The black dashed line represents the ΛCDM model corresponding to $b = 0$.

growth factors combined with CMB+BAO+SNe+GRB observations (Xia 2009), $\Omega_{\rm m} = 0.235^{+0.125}_{-0.074}$ given by galaxy clusters combined with SNe+GRBs+CMB+BAO+OHD observations (Liang & Zhu 2011), and $\Omega_{\rm m} = 0.243^{+0.077}_{-0.074}$ given by strong gravitational lensing systems (Ma et al. 2019). For comparison, the fitting results from the combined QSO[XUV]+QSO[AS]+BAO data sets are also shown in Fig. 3, with the matter density parameter of $\Omega_{\rm m} = 0.329^{+0.009}_{-0.009}$. The use of BAO data to constrain cosmological models

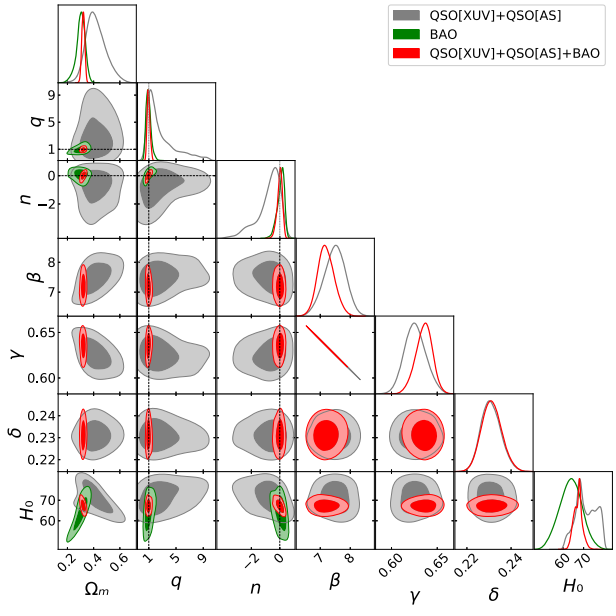

Figure 6. The 1D probability distributions and 2D contours with 1σ and 2σ confidence levels for MPC model, obtained from QSO[XUV]+QSO[AS] (grey), BAO (green), and QSO[XUV]+QSO[AS]+BAO (red) data. The black dashed line indicates the ΛCDM model corresponding to $q = 1$ and $n = 0$.

seems to be complementary to the QSO distance measurements, considering the constrained results especially on $\Omega_{\rm m}$ and H_0.

5.2 Observational constraints on generalized Chaplygin gas model

Fig. 4 and Table 2 present the results of the best-fitting parameters for the GCG model. One can see a deviation between the constraints of ($\Omega_{\rm m}$, α, H_0) coming from the three combined data sets, which are still consistent with each other within 2σ confidence level. On the one hand, the combined data sets QSO[XUV]+QSO[AS] cannot tightly constrain the model parameters ($\Omega_{\rm m}$, α), especially for parameter α whose best-fitting value is $\alpha = 2.360^{+1.803}_{-1.793}$ and $\Omega_{\rm m}$ is much larger than the value implied by other measurements. In the framework of GCG, considering the fact that the parameter α quantifies the deviation from the ΛCDM model and the SCG model, ΛCDM is not consistent with GCG at 1σ confidence level, while SCG is more favoured by the QSO[XUV]+QSO[AS] data. However, in the case of BAO and QSO[XUV]+QSO[AS]+BAO data, ΛCDM is still favoured within 1σ, with $\alpha = -0.227^{+0.272}_{-0.246}$ and $\alpha = -0.067^{+0.151}_{-0.147}$, respectively. The combined data set of QSO[XUV]+QSO[AS]+BAO provides more stringent constraints on the matter density parameter ($\Omega_{\rm m} = 0.319^{+0.010}_{-0.009}$) and the Hubble constant ($H_0 = 67.496^{+1.605}_{-1.904}\,{\rm km\,s^{-1}\,Mpc^{-1}}$). For comparison, the results obtained from the joint light-curve analysis (JLA) compilation of SNe Ia, CMB, BAO, and 30 OHD data simulated over redshift range $2 \leq z \leq 5$ gave $\Omega_{\rm m} = 0.345^{+0.006}_{-0.006}$ and $\alpha = -0.047^{+0.027}_{-0.026}$ (Liu et al. 2019b), which prefers a higher value of $\Omega_{\rm m}$ than our results and does not include ΛCDM within 1σ range. It is interesting to note that Liu et al. (2019b) also obtained $\alpha = -0.040^{+0.060}_{-0.065}$ without adding the simulated data, which still includes the ΛCDM model at 1σ confidence level and is slightly different from the results obtained by adding the simulated higher redshift. This may indicate that the data within the 'redshift desert' ($2 \leq z \leq 5$) can provide a valuable

Table 2. Summary of the best-fitting values with their 1σ uncertainties concerning the parameters of all considered models. The results are obtained from the combined data sets of QSO[XUV]+QSO[AS], BAO, and QSO[XUV]+QSO[AS]+BAO.

Model	Data	Ω_m	β	γ	δ	H_0		
ΛCDM	QSO[XUV]+QSO[AS]	$0.406^{+0.108}_{-0.082}$	$7.321^{+0.308}_{-0.314}$	$0.631^{+0.010}_{-0.010}$	$0.231^{+0.004}_{-0.004}$	$64.704^{+3.347}_{-3.744}$		
	BAO	$0.316^{+0.022}_{-0.020}$	–	–	–	$68.074^{+1.545}_{-1.380}$		
	QSO[XUV]+QSO[AS]+BAO	$0.317^{+0.007}_{-0.007}$	$7.152^{+0.265}_{-0.260}$	$0.637^{+0.009}_{-0.009}$	$0.231^{+0.004}_{-0.004}$	$68.157^{+0.496}_{-0.487}$		
DGP	QSO[XUV]+QSO[AS]	$0.365^{+0.129}_{-0.100}$	$7.358^{+0.328}_{-0.309}$	$0.630^{+0.010}_{-0.010}$	$0.231^{+0.004}_{-0.004}$	$62.353^{+3.877}_{-3.709}$		
	BAO	$0.269^{+0.022}_{-0.020}$	–	–	–	$59.560^{+1.149}_{-1.004}$		
	QSO[XUV]+QSO[AS]+BAO	$0.329^{+0.009}_{-0.009}$	$7.299^{+0.263}_{-0.271}$	$0.632^{+0.009}_{-0.009}$	$0.231^{+0.004}_{-0.004}$	$62.757^{+0.488}_{-0.471}$		
			α	β	γ	δ	H_0	
GCG	QSO[XUV]+QSO[AS]	$0.416^{+0.088}_{-0.068}$	$2.360^{+1.803}_{-1.793}$	$7.419^{+0.326}_{-0.340}$	$0.628^{+0.011}_{-0.011}$	$0.231^{+0.004}_{-0.004}$	$69.254^{+4.427}_{-4.970}$	
	BAO	$0.299^{+0.029}_{-0.039}$	$-0.227^{+0.272}_{-0.246}$	–	–	–	$63.972^{+5.266}_{-5.866}$	
	QSO[XUV]+QSO[AS]+BAO	$0.319^{+0.010}_{-0.009}$	$-0.067^{+0.151}_{-0.147}$	$7.186^{+0.259}_{-0.250}$	$0.636^{+0.008}_{-0.009}$	$0.231^{+0.005}_{-0.004}$	$67.496^{+1.605}_{-1.904}$	
			b	β	γ	δ	H_0	
$f(T)$	QSO[XUV]+QSO[AS]	$0.409^{+0.131}_{-0.090}$	$-0.193^{+0.551}_{-0.509}$	$7.344^{+0.313}_{-0.331}$	$0.631^{+0.011}_{-0.010}$	$0.231^{+0.005}_{-0.005}$	$63.829^{+4.147}_{-4.839}$	
	BAO	$0.303^{+0.028}_{-0.029}$	$0.261^{+0.252}_{-0.323}$	–	–	–	$64.154^{+4.806}_{-4.858}$	
	QSO[XUV]+QSO[AS]+BAO	$0.320^{+0.010}_{-0.009}$	$0.084^{+0.176}_{-0.166}$	$7.163^{+0.280}_{-0.269}$	$0.637^{+0.009}_{-0.009}$	$0.231^{+0.005}_{-0.004}$	$67.507^{+1.327}_{-1.987}$	
			q	n	β	γ	δ	H_0
MPC	QSO[XUV]+QSO[AS]	$0.410^{+0.085}_{-0.062}$	$1.936^{+2.923}_{-0.982}$	$-0.547^{+0.564}_{-0.981}$	$7.497^{+0.343}_{-0.374}$	$0.626^{+0.012}_{-0.011}$	$0.231^{+0.005}_{-0.004}$	$70.576^{+6.475}_{-4.435}$
	BAO	$0.304^{+0.030}_{-0.034}$	$0.914^{+0.381}_{-0.322}$	$0.120^{+0.192}_{-0.320}$	–	–	–	$63.800^{+5.177}_{-5.620}$
	QSO[XUV]+QSO[AS]+BAO	$0.321^{+0.011}_{-0.011}$	$0.944^{+0.237}_{-0.183}$	$0.022^{+0.165}_{-0.205}$	$7.176^{+0.290}_{-0.253}$	$0.636^{+0.008}_{-0.010}$	$0.231^{+0.005}_{-0.005}$	$67.462^{+1.663}_{-2.324}$

supplement to other astrophysical observations in the framework of GCG model.

5.3 Observational constraints on power-law $f(T)$ model

In the case of $f(T)$ theory based on $f(T) = \alpha(-T)^b$ ansatz, the results are presented in Fig. 5 and can be seen in Table 2. It can be clearly seen from the comparison plots, there is a consistency between QSO[XUV]+QSO[AS], BAO, and QSO[XUV]+QSO[AS]+BAO. However, the QSO[XUV]+QSO[AS] data generate a higher matter density parameter $\Omega_m = 0.409^{+0.131}_{-0.090}$ compared with other probes. As for the parameter b that captures the deviation of the $f(T)$ model from the ΛCDM model, the best-fitting value is $b = -0.193^{+0.551}_{-0.509}$ and the ΛCDM model ($b = 0$) is still included within 1σ range. Such conclusion could also be carefully derived in the case of BAO and QSO[XUV]+QSO[AS]+BAO measurements. For comparison, our results are similar to the results obtained with QSO(AS)+SNe Ia+BAO+CMB data sets ($\Omega_m = 0.317 \pm 0.010$, $b = 0.057^{+0.091}_{-0.065}$; Qi et al. 2017) and SNe Ia+BAO+CMB+dynamical growth data ($\Omega_m = 0.272 \pm 0.008$, $b = -0.017 \pm 0.083$; Nesseris et al. 2013), where the value of Ω_m is in tension with our results within 1σ. Moreover, in the framework of the power-law $f(T)$ model, the parameter b obtained from QSO[XUV]+QSO[AS] and BAO alone seems to deviate from zero more according to the above-mentioned results, which suggests that there are still some possibility that ΛCDM may not be the best cosmological model preferred by current observations with larger redshift range. With the combined data sets QSO[XUV]+QSO[AS]+BAO, we also get stringent constraints on the model parameters $\Omega_m = 0.320^{+0.009}_{-0.010}$, $b = 0.084^{+0.176}_{-0.166}$, and $H_0 = 67.507^{+1.327}_{-1.987}$ km s^{-1} Mpc^{-1}, where ΛCDM is included within 1σ. It is worth noting that this slight deviation from the ΛCDM is also in agreement with similar results in the literature, obtained from QSO[AS]+BAO+CMB ($b = 0.080 \pm 0.077$; Qi et al. 2017) and OHD+SNe Ia+BAO+CMB ($b = 0.05128^{+0.025}_{-0.019}$; Nunes, Pan & Saridakis 2016).

5.4 Observational constraints on modified polytropic Cardassian model

All values of the estimated cosmic parameters in the MPC model are displayed in Table 2 and illustrated in Fig. 6. For the QSO[XUV]+QSO[AS], BAO, and QSO[XUV]+QSO[AS]+BAO data, the best-fitting values of the parameters (q and n) are in good agreement with each other within 2σ. Meanwhile, ΛCDM is still favoured by the current QSO and BAO measurements within 1σ confidence level in the MPC model. Apparently, however, the combined QSO data support higher matter density parameter $\Omega_m = 0.410^{+0.085}_{-0.062}$ than that from the other two data sets within 68.3 per cent confidence level. The constraints on the parameters q and n from the QSO[XUV]+QSO[AS] data are very weak: $q = 1.936^{+2.923}_{-0.982}$, $n = -0.547^{+0.564}_{-0.981}$, but it seems that the central values of q and n deviate more from 1 and 0, respectively, in comparison to the results obtained with BAO and QSO[XUV]+QSO[AS]+BAO. This may suggest that the quasar data (especially QSO[XUV]) at higher redshift may have some possibility of favouring the modifications to the Friedmann equations in the MPC model. Several authors have tested the MPC model with different measurements. For instance, the SNe Ia+BAO+CMB+OHD data sets gave $q = 0.897^{+0.152}_{-0.468}$, $n = -0.648^{+0.856}_{-1.106}$ (Shi et al. 2012), which are in good accordance with our results obtained of the BAO measurements and QSO[XUV]+QSO[AS]+BAO. In addition, our limits are similar to $q = 3.29 \pm 3.30$, $n = 0.26 \pm 0.13$ shown in Magana et al. (2015) using BAO data, and in tension with the results obtained from strong lensing measurements (Magana et al. 2015) in Abell 1689: $q = 5.2 \pm 2.25$, $n = 0.41 \pm 0.25$. With the Supernova Legacy Survey 3-year sample (SNLS3) SN Ia sample+CMB+BAO+OHD data sets, Li, Wu & Yu (2012) got the constraints $q = 1.098^{+1.015}_{-0.465}$

Table 3. Information theoretic model comparison. Minimum values of AIC, BIC, and their differences and weights are reported for the ΛCDM and each of the four cosmological models considered. Jensen–Shannon divergence $D_{\rm JS}$ between ΛCDM and other cosmological models was calculated with respect to the matter density parameter $\Omega_{\rm m}$ and the Hubble constant H_0.

Data	Model	AIC	ΔAIC	ω_i(AIC)	BIC	ΔBIC	ω_i(BIC)	$\chi^2_{\rm min}$/dof	$D_{\rm JS}(\Omega_{\rm m})$	$D_{\rm JS}(H_0)$
QSO[XUV]+QSO[AS]	ΛCDM	2217.95	1.25	0.257	2245.19	1.25	0.3419	1.289	0	0
	DGP	2216.70	0	0.479	2243.94	0	0.6376	1.288	0.233	0.273
	GCG	2218.58	1.88	0.188	2251.27	7.32	0.0164	1.289	0.199	0.447
	$f(T)$	2221.43	4.73	0.045	2254.12	10.18	0.0039	1.291	0.161	0.136
	MPC	2222.20	7.38	0.031	2260.34	16.40	0.0002	1.291	0.224	0.516
BAO	ΛCDM	13.88	1.57	0.233	14.68	1.57	0.2454	1.098	0	0
	DGP	12.32	0	0.511	13.11	0	0.5370	0.924	0.749	0.999
	GCG	15.95	3.63	0.083	17.14	4.03	0.0716	1.244	0.339	0.658
	$f(T)$	14.71	2.39	0.155	15.90	2.79	0.1332	1.090	0.270	0.640
	MPC	18.99	1.57	0.018	20.59	7.47	0.0128	1.571	0.255	0.663
QSO[XUV]+QSO[AS]+BAO	ΛCDM	2227.20	0	0.780	2254.47	0	0.9483	1.286	0	0
	DGP	2233.63	6.43	0.031	2260.90	6.43	0.0381	1.289	0.566	0.999
	GCG	2230.45	3.25	0.153	2263.18	8.71	0.0122	1.288	0.198	0.586
	$f(T)$	2234.92	7.72	0.016	2267.65	13.18	0.0013	1.290	0.214	0.547
	MPC	2234.58	7.38	0.020	2272.77	18.30	0.0001	1.290	0.322	0.629

and $n = 0.014^{+0.364}_{-0.946}$, which is consistent with our limits. Note that also with the QSO[XUV]+QSO[AS]+BAO data sets the best-fitting values of q and n parameters deviate from 1 and 0, respectively, which implies the possibility of the modifications to the Friedmann equations.

From our constraints on the matter density parameter $\Omega_{\rm m}$ in different non-standard cosmological models, one thing is quite clear that the combined QSO data containing large number of measurements at high redshifts ($2 \leq z \leq 5$) do favour $\Omega_{\rm m}$ lying in the range from $0.365^{+0.129}_{-0.100}$ to $0.416^{+0.088}_{-0.068}$. This is considerably higher than the constraints from other probes (such as BAO measurements). Actually, such results on $\Omega_{\rm m}$ have been noted in the previous works through different approaches. For instance, Khadka & Ratra (2020b) obtained $\Omega_{\rm m} \sim 0.5$–0.6 in four different cosmological models with large number of QSO[XUV], while Qi et al. (2017) derived $\Omega_{\rm m} = 0.319 \pm 0.011$ and $\Omega_{\rm m} = 0.329 \pm 0.011$ in different $f(T)$ theories with QSO[AS]+BAO+CMB data sets. Other studies of different DE models (based on Pade approximation parametrizations) revealed the similar conclusions with Pantheon+GRB+QSO: the matter density parameter lies in the range from $\Omega_{\rm m} = 0.384^{+0.033}_{-0.022}$ to $\Omega_{\rm m} = 0.391^{+0.038}_{-0.026}$ (Rezaei et al. 2020). Meanwhile, some recent studies (Benetti & Capozziello 2019; Lusso et al. 2019; Risaliti & Lusso 2019; Demianski et al. 2020; Rezaei et al. 2020; Yang, Banerjee & Ó Colgáin 2020; Li et al. 2021) focused on exploring the deviation between high-redshift measurements and the standard cosmological model. In spite of the $\Omega_{\rm m}$ inconsistency obtained from the measurements with different redshift coverage, it is still under controversy whether this is an indication of a new physics or an unknown systematic effect of the high-redshift observations. Therefore, besides developing new high quality and independent cosmological probes, it would be more interesting to figure out why the standard cosmological parameters are fitted to different values with high- and low-redshift observations. The latter indicates that one could go beyond ΛCDM model to properly describe our universe (Ding et al. 2015; Zheng et al. 2016).

As for the constraints on the Hubble constant H_0 shown in Table 2, one can see that H_0 lies in the range from $H_0 = 62.353^{+3.877}_{-3.709}$ to $H_0 = 70.576^{+6.475}_{-4.435}\,{\rm km\,s^{-1}\,Mpc^{-1}}$ for the combined QSO data, from $H_0 = 59.560^{+1.149}_{-1.004}$ to $H_0 = 68.074^{+1.545}_{-1.380}\,{\rm km\,s^{-1}\,Mpc^{-1}}$ for BAO, and from $H_0 = 62.757^{+0.488}_{-0.471}$ to $H_0 = 68.157^{+0.496}_{-0.487}\,{\rm km\,s^{-1}\,Mpc^{-1}}$ for QSO[XUV]+QSO[AS]+BAO. Apparently, almost all the results for H_0 are lower than 70 km s^{-1} Mpc^{-1}, except for the MPC model assessed with QSO[XUV]+QSO[AS] that however has large uncertainties.

5.5 Model comparison

In this section, we compare the models and discuss how strongly are they supported by the observational data sets. In Table 3 one can find the summary of the information theoretical model selection criteria applied to different models from QSO[XUV]+QSO[AS], BAO, and QSO[XUV]+QSO[AS]+BAO data sets. It can be seen that ΛCDM is still the best model for the combined data QSO[XUV]+QSO[AS]+BAO, under the assessment of AIC and BIC. Although the quasar sample (QSO[XUV]+QSO[AS]) and the BAO data tend to prefer the DGP model in term of AIC and BIC, they also share the same preference for ΛCDM, compared with other theories of modified gravity.

It is important to keep in mind that model selection provides a quantitative information on the strength of evidence (or the degree of support) rather than just selecting only one model (Lu et al. 2008). Table 3 informs us that AIC applied to the QSO[XUV]+QSO[AS] data set does not effectively discriminate ΛCDM and GCG models – both of them receive the similar support, while the evidence against $f(T)$ and MPC model is very strong. For the QSO[XUV]+QSO[AS]+BAO data, we find that the DGP, $f(T)$, and MPC model are clearly disfavoured by the data, as they are unable to provide a good fit. The BIC diversifies the evidence between the models. Out of all the candidate models, it is obvious that models with more free parameters (GCG, $f(T)$, and MPC) are less favoured by the current quasar observations (QSO[XUV]+QSO[AS]). Among these four modified gravity models, the evidence against MPC is very noticeable for all kinds of data sets, which demonstrates the MPC model is seriously punished by the BIC.

Traditional information criteria (AIC or BIC) do not provide much insight into the agreement between ΛCDM and the other four models. Therefore, we also calculated the JSD (see Section 4.4) in order to assess which models are consistent with ΛCDM in light of the observational data. As already mentioned one should have common parameters in all compared models and we used in

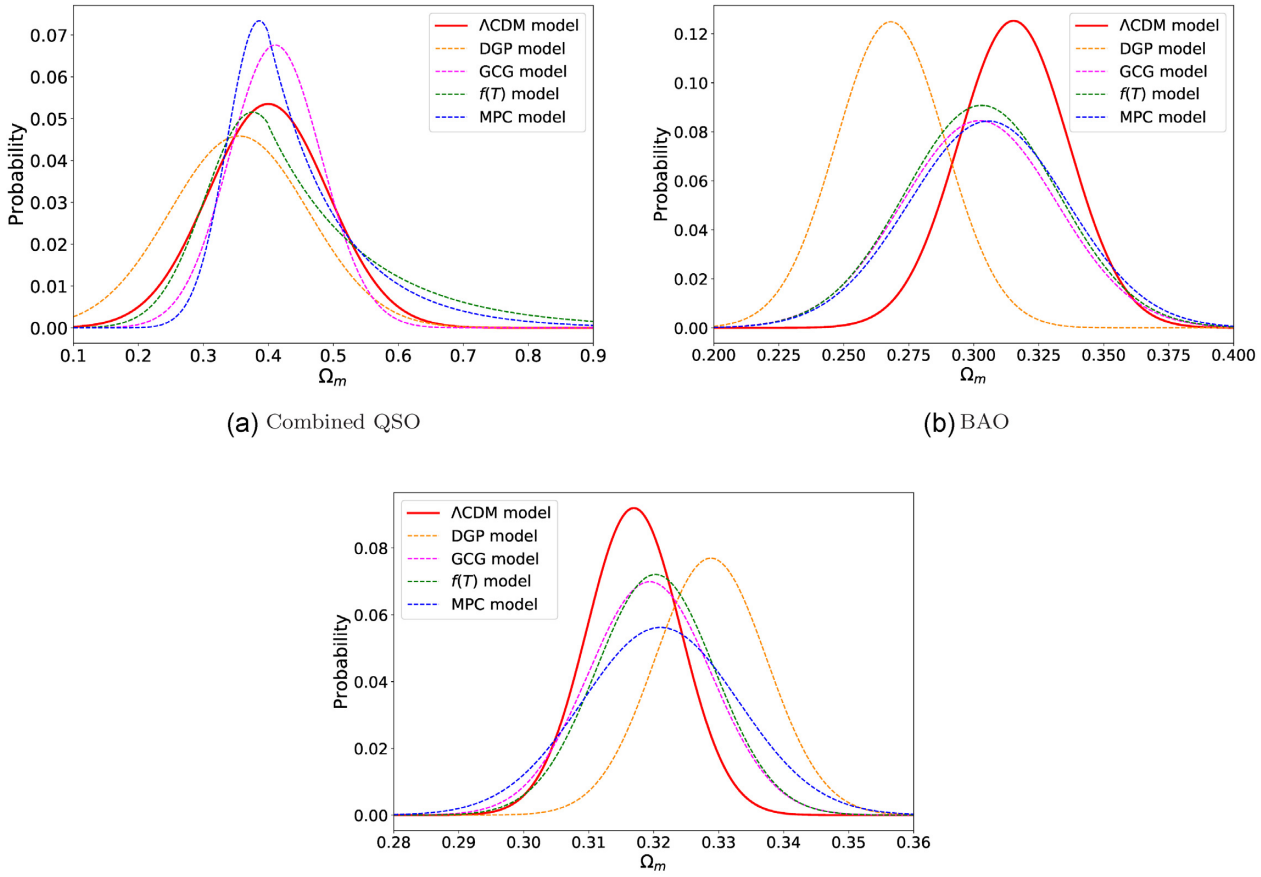

Figure 7. The posterior distributions of $\Omega_{\rm m}$ for ΛCDM, DGP, GCG, $f(T)$, and MPC model, with the combined QSO, BAO, and combined QSO+BAO data.

this role the matter density parameter and Hubble constant. Figs 7 and 8 show the posterior distribution of $\Omega_{\rm m}$ and H_0 obtained with QSO[XUV]+QSO[AS], BAO, and QSO[XUV]+QSO[AS]+BAO data sets for all models considered. For QSO[XUV]+QSO[AS] data, the posterior distributions of $\Omega_{\rm m}$ and H_0 in $f(T)$ models agree more with that of ΛCDM in terms of the value of JSD. As for the BAO measurements, the value of JSD concerning $\Omega_{\rm m}$ shows the MPC model agrees more with the ΛCDM, but concerning H_0, all four non-standard models give large distance from the ΛCDM, where the $f(T)$ model is still the closest to it. In the case of QSO[XUV]+QSO[AS]+BAO data sets, the DGP and MPC model are much more distant from the ΛCDM for the posterior distributions of $\Omega_{\rm m}$, while GCG and $f(T)$ models are closer to it, which is similar to the cases for the posterior distributions of H_0.

6 CONCLUSIONS

The modified gravity could provide interesting approaches to explain the cosmic acceleration, without involving DE. In this paper, we have evaluated the power of multiple measurements of quasars covering sufficiently wide redshift range, on constraining some popular modified gravity theories including DGP, GCG, the power-law $f(T)$ model, and MPC model, under the assumption of the spatial flatness of the Universe. As for the observational data, the newest large sample of QSO X-ray and UV flux measurements (Risaliti & Lusso 2019) was used as standard candles and provided a good opportunity to test models at the 'redshift desert' ($2 \leq z \leq 5$) that is not yet widely available through other observations. In addition, a popular compilation of 120 angular size measurements of compact structure in radio quasars versus redshift data from the VLBI over the redshift range $0.46 < z < 2.76$ (Cao et al. 2017b) was used as standard rulers to test these models in conjunction with the 1598 QSO X-ray and UV flux measurements. Meanwhile, with the aim to tighten the constraint from the combined QSO data sets and test the consistency with other observations, 11 recent BAO measurements in the redshift range $0.122 \leq z \leq 2.34$ (Cao et al. 2020b) were also taken into account in this work. Here we summarize our main conclusions in more detail.

(i) Our results show that calibrating parameters β and γ from the non-linear $L_{\rm X}$–$L_{\rm UV}$ relation and the global intrinsic dispersion δ are almost independent of the cosmological model, which is similar to the results from Khadka & Ratra (2020b). This supports the evidence that these selected quasars can be regarded as standard candles.

(ii) In all four non-standard cosmological models, the results show that the combined QSO data alone are not able to provide tight constraints on model parameters, which is mainly related to the large dispersion ($\delta = 0.23$) of the $L_{\rm X}$–$L_{\rm UV}$ relation obtained from the 1598 QSO X-ray and UV flux measurements. On the other hand, the combined quasar data constraints are mostly coherent with the joint analysis including BAO measurements. The value of matter density parameter $\Omega_{\rm m}$ implied by the combined QSO data is noticeably larger than that derived from other measurements, which is likely caused by the discrepancy between the QSO X-ray and UV flux data

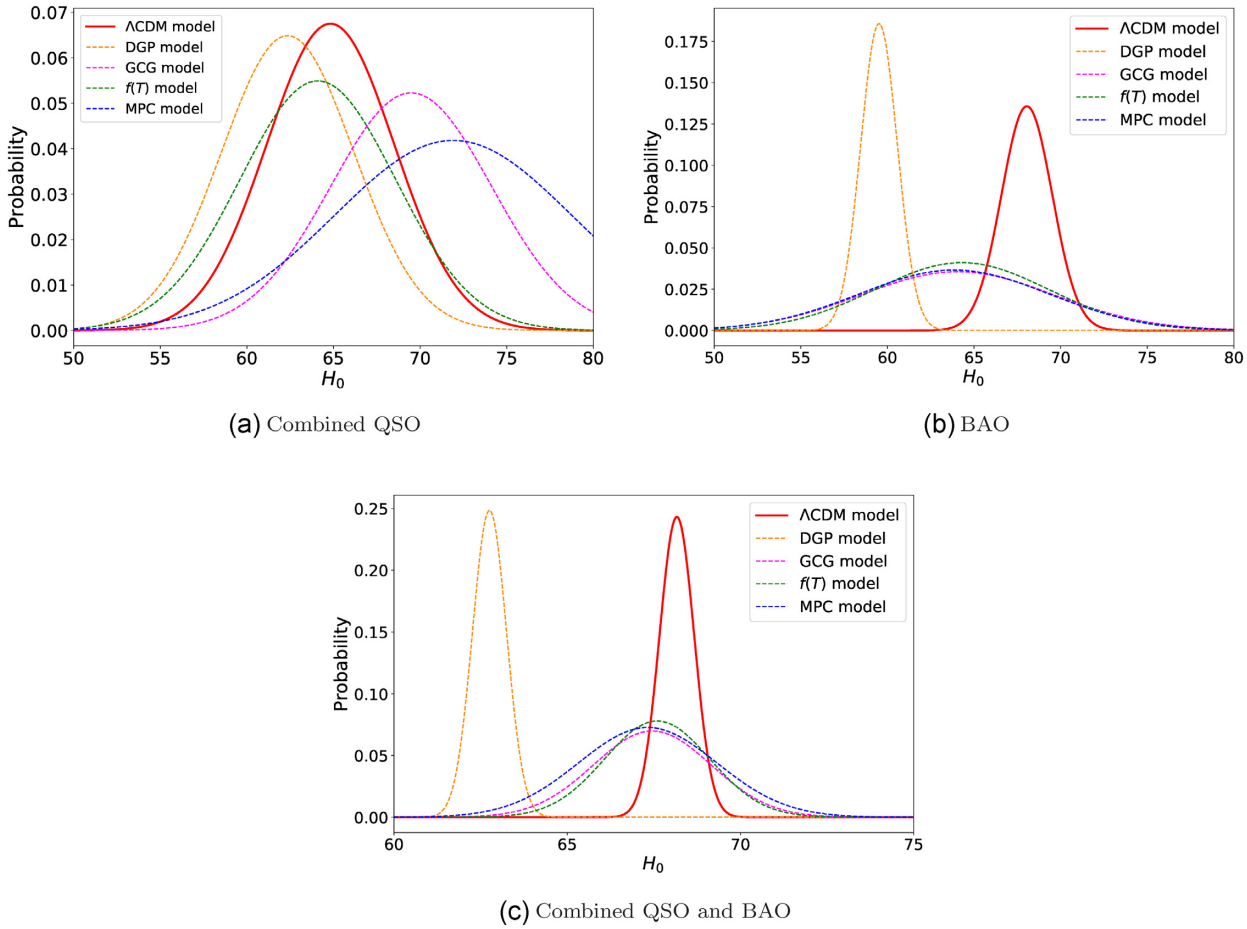

Figure 8. The posterior distributions of H_0 for ΛCDM, DGP, GCG, $f(T)$, and MPC model, with the combined QSO, BAO, and combined QSO+BAO data.

and the $\Omega_m = 0.3$ flat ΛCDM (Risaliti & Lusso 2019; Khadka & Ratra 2020b). It is quite possible that quasar data at high redshifts can shed new light on the model of our universe. Moreover, in this paper, we tested different alternative models. Most of them include the concordance ΛCDM model as a special case corresponding to certain values of their parameters, such as the parameter b in the power-law $f(T)$ model. For the $f(T)$ and MPC model, ΛCDM turned out to be compatible with them at 1σ confidence level, while the GCG model is generally inconsistent with the cosmological constant case within 1σ. Furthermore, after including BAO in the joint analysis, the best-fitting value of these parameters and their 1σ confidence levels show less deviation from ΛCDM, which suggests that BAO measurements favour ΛCDM significantly.

(iii) According to the AIC and BIC, the concordance ΛCDM model is still the best cosmological model in light of the combined QSO and BAO data, while the MPC model has considerably less support as the best one. Although the quasar sample (QSO[XUV]+QSO[AS]) and the BAO data tend to prefer the DGP model in term of AIC and BIC, they also share the same preference for ΛCDM, compared with other theories of modified gravity. Therefore, non-standard models with more free parameters are less favoured by the available observations, which is the most unambiguous result of the current data set. In order to compare the agreement between the ΛCDM model and other four models, JSD was applied in this paper. We found that for the combined QSO data, the posterior distribution of Ω_m and H_0 from $f(T)$ was in a better agreement with ΛCDM. For BAO measurements, MPC and $f(T)$ models are closer to ΛCDM according to the values of JSD from the posterior distribution of Ω_m, while all four models are distant from ΛCDM in the case of H_0, especially the DGP model. With QSO+BAO data, the results are similar to that from BAO measurements, but the posterior distribution of Ω_m from GCG and $f(T)$ model is in better agreement with ΛCDM.

ACKNOWLEDGEMENTS

This work was supported by the National Natural Science Foundation of China under Grant Nos 12021003, 11690023, 11633001, and 11920101003, the National Key Research and Development Program of China (Grant No. 2017YFA0402600), the Beijing Talents Fund of Organization Department of the Beijing Municipal Committee of the Communist Party of China, the Strategic Priority Research Program of the Chinese Academy of Sciences (Grant No. XDB23000000), the Interdiscipline Research Funds of Beijing Normal University, and the Opening Project of Key Laboratory of Computational Astrophysics, National Astronomical Observatories, Chinese Academy of Sciences. MB was supported by the Foreign Talent Introducing Project and Special Fund Support of Foreign Knowledge Introducing Project in China. He was also supported by the Key Foreign Expert Program for the Central Universities No. X2018002.

DATA AVAILABILITY

The data underlying this paper will be shared on reasonable request to the corresponding author.

REFERENCES

Abbott B. P. et al., 2019a, Phys. Rev. X, 9, 031040
Abbott T. M. C. et al., 2019b, MNRAS, 483, 4866
Akaike H., 1974, IEEE Trans. Automatic Control, AC-19, 716
Alam S. et al., 2017, MNRAS, 470, 2617
Allen S. W., Rapetti D. A., Schmidt R. W., Ebeling H., Morris R. G., Fabian A. C., 2008, MNRAS, 383, 879
Amante M. H., Magaña J., Motta V., García-Aspeitia M. A., Verdugo T., 2020, MNRAS, 498, 6013
Amendola L., 2000, Phys. Rev. D, 62, 043511
Ata M. et al., 2018, MNRAS, 473, 4773
Avni Y., Tananbaum H., 1986, ApJ, 305, 83
Baldwin J. A., 1977, ApJ, 214, 679
Benetti M., Capozziello S., 2019, J. Cosmol. Astropart. Phys., 12, 008
Bengochea G. R., Ferraro R., 2009, Phys. Rev. D, 79, 124019
Bento M. C., Bertolami O., Sen A. A., 2002, Phys. Rev. D, 66, 043507
Biesiada M., 2007, J. Cosmol. Astropart. Phys., 02, 003
Biesiada M., Godłowski W., Szydłowski M., 2005, ApJ, 622, 28
Biesiada M., Malec B., Piorkowska A., 2011, Res. Astron. Astrophys., 11, 641
Bisogni S., Risaliti G., Lusso E., 2017, Frontiers Astron. Space Sci., 4, 68
Boisseau B., Esposito-Farese G., Polarski D., Starobinsky A. A., 2000, Phys. Rev. Lett., 85, 2236
Bonamente M., Joy M. K., LaRoque S. J., Carlstrom J. E., Reese E. D., Dawson K. S., 2006, ApJ, 647, 25
Cai Y.-F., Capozziello S., De Laurentis M., Saridakis E. N., 2016, Rep. Progress Phys., 79, 106901
Caldera-Cabral G., Maartens R., Urena-Lopez L. A., 2009, Phys. Rev. D, 79, 063518
Caldwell R. R., Linder E. V., 2005, Phys. Rev. Lett., 95, 141301
Cao S., Zhu Z.-H., 2012, A&A, 538, A43
Cao S., Zhu Z.-H., Zhao R., 2011, Phys. Rev. D, 84, 023005
Cao S., Pan Y., Biesiada M., Godlowski W., Zhu Z.-H., 2012a, J. Cosmol. Astropart. Phys., 03, 016
Cao S., Covone G., Zhu Z.-H., 2012b, ApJ, 755, 31
Cao S., Biesiada M., Gavazzi R., Piórkowska A., Zhu Z.-H., 2015, ApJ, 806, 185
Cao S., Biesiada M., Jackson J., Zheng X., Zhao Y., Zhu Z.-H., 2017a, J. Cosmol. Astropart. Phys., 02, 012
Cao S., Zheng X., Biesiada M., Qi J., Chen Y., Zhu Z.-H., 2017b, A&A, 606, A15
Cao S., Li X., Biesiada M., Xu T., Cai Y., Zhu Z.-H., 2017c, ApJ, 835, 92
Cao S., Biesiada M., Qi J., Pan Y., Zheng X., Xu T., Ji X., Zhu Z.-H., 2018, Eur. Phys. J. C, 78, 749
Cao S., Qi J., Biesiada M., Zheng X., Xu T., Pan Y., Zhu Z.-H., 2019, Phys. Dark Universe, 24, 100274
Cao S., Qi J., Biesiada M., Liu T., Zhu Z.-H., 2020a, ApJ, 888, L25
Cao S. L., Ryan J., Ratra B., 2020b, MNRAS, 497, 3191
Carter P., Beutler F., Percival W. J., Blake C., Koda J., Ross A. J., 2018, MNRAS, 481, 2371
Chen G., Ratra B., 2003, ApJ, 582, 586
Chen Y., Ratra B., 2011, Phys. Lett. B, 703, 406
Chen Y., Ratra B., 2012, A&A, 543, A104
Chen Y., Geng C.-Q., Cao S., Huang Y.-M., Zhu Z.-H., 2015, J. Cosmol. Astropart. Phys., 02, 010
Chen Y., Ratra B., Biesiada M., Li S., Zhu Z.-H., 2016, ApJ, 829, 61
Chiba T., 2003, Phys. Lett. B, 575, 1
Clifton T., Ferreira P. G., Padilla A., Skordis C., 2012, Phys. Rep., 513, 1
Cooke R. J., Pettini M., Steidel C. C., 2018, ApJ, 855, 102
Copeland E. J., Sami M., Tsujikawa S., 2006, Int. J. Mod. Phys. D, 15, 1753
De Bernardis F., Giusarma E., Melchiorri A., 2006, Int. J. Mod. Phys. D, 15, 759
Demianski M., Lusso E., Paolillo M., Piedipalumbo E., Risaliti G., 2020, Frontiers Astron. Space Sci., 7, 69
de Sainte Agathe V. et al., 2019, A&A, 629, A85
Ding X., Biesiada M., Cao S., Li Z., Zhu Z.-H., 2015, ApJ, 803, L22
Dvali G., Gabadadze G., Porrati M., 2000, Phys. Lett. B, 485, 208
Eisenstein D. J., Hu W., 1998, ApJ, 496, 605
Eisenstein D. J. et al., 2005, ApJ, 633, 560
Farooq O., Madiyar F., Crandall S., Ratra B., 2017, ApJ, 835, 26
Foreman-Mackey D., Hogg D. W., Lang D., Goodman J., 2013, PASP, 125, 306
Freese K., Lewis M., 2002, Phys. Lett. B, 540, 1
Geng S., Cao S., Liu T., Biesiada M., Qi J., Liu Y., Zhu Z.-H., 2020, ApJ, 905, 54
Ghirlanda G., Ghisellini G., Firmani C., 2006, New J. Phys., 8, 123
Gondolo P., Freese K., 2002, preprint (arXiv:hep-ph/0211397)
Gurvits L., 1994, ApJ, 425, 442
Gurvits L. I., Kellermann K. I., Frey S., 1999, A&A, 342, 378
Kamenshchik A. Yu., Moschella U., Pasquier V., 2001, Phys. Lett. B, 511, 265
Kellermann K., 1993, Nature, 361, 134
Khadka N., Ratra B., 2020a, MNRAS, 492, 4456
Khadka N., Ratra B., 2020b, MNRAS, 497, 263
Koyama K., 2016, Rep. Progress Phys., 79, 046902
Lamb D. Q., Reichart D. E., 2000, ApJ, 536, 1
Li Z., Wu P., Yu H., 2012, ApJ, 744, 176
Li Z., Liao K., Wu P., Yu H., Zhu Z. H., 2013, Phys. Rev. D, 88, 023003
Li X., Cao S., Zheng X., Qi J., Biesiada M., Zhu Z.-H., 2017, Eur. Phys. J. C, 77, 677
Li X., Keeley R. E., Shafieloo A., Zheng X., Cao S., Biesiada M., Zhu Z.-H., 2021, preprint (arXiv:2103.16032)
Liang E., Zhang B., 2005, ApJ, 633, 611
Liang N., Zhu Z.-H., 2011, Res. Astron. Astrophys., 11, 497
Lin J., 1991, IEEE Trans. Inf. Theory, 37, 145
Liu T., Cao S., Zhang J., Geng S., Liu Y., Ji X., Zhu Z.-H., 2019a, ApJ, 886, 94
Liu Y., Guo R.-Y., Zhang J.-F., Zhang X., 2019b, J. Cosmol. Astropart. Phys., 05, 016
Liu T., Cao S., Zhang J., Biesiada M., Liu Y., Lian Y., 2020a, MNRAS, 496, 708
Liu T., Cao S., Biesiada M., Liu Y., Geng S., Lian Y., 2020b, ApJ, 899, 71
Liu Y., Cao S., Liu T., Li X., Geng S., Lian Y., Guo W., 2020c, ApJ, 901, 129
Lu J., Xu L., Liu M., Gui Y., 2008, Eur. Phys. J. C, 58, 311
Lusso E., Risaliti G., 2016, ApJ, 819, 154
Lusso E., Piedipalumbo E., Risaliti G., Paolillo M., Bisogni S., Nardini E., Amati L., 2019, A&A, 628, L4
Ma Y.-B., Cao S., Zhang J., Geng S., Liu Y., Liu T., Pan Y., 2019, Eur. Phys. J. C, 79, 121
Magana J., Motta V., Cardenas V. H., Verdugo T., Jullo E., 2015, ApJ, 813, 69
Malekjani M., Khodam-Mohammadi A., Nazari-pooya N., 2011, Ap&SS, 334, 193
Maor I., Brustein R., Steinhardt P. J., 2001, Phys. Rev. Lett., 86, 6
Melia Y., Zhang J., Cao S., Zheng X., Xu T., Qi J., 2017, Eur. Phys. J. C, 77, 891
Nesseris S., Perivolaropoulos L., 2005, Phys. Rev. D, 72, 123519
Nesseris S., Basilakos S., Saridakis E. N., Perivolaropoulos L., 2013, Phys. Rev. D, 88, 103010
Nojiri S., Odintsov S. D., 2005, Phys. Lett. B, 631, 1
Nunes R. C., Pan S., Saridakis E. N., 2016, J. Cosmol. Astropart. Phys., 08, 011
Peebles P. J. E., Ratra B., 1988, ApJ, 325, L17
Percival W. J., Cole S., Eisenstein D. J., Nichol R. C., Peacock J. A., Pope A. C., Szalay A. S., 2007, MNRAS, 381, 1053
Perlmutter S. et al., 1999, ApJ, 517, 565
Planck Collaboration XIII, 2016, A&A, 594, A13
Planck Collaboration VI, 2020, A&A, 641, A6
Plionis M., Terlevich R., Basilakos S., Bresolin F., Terlevich E., Melnick J., Chavez R., 2011, MNRAS, 416, 2981
Qi J.-Z., Cao S., Biesiada M., Zheng X., Zhu Z.-H., 2017, Eur. Phys. J. C, 77, 502
Qi J.-Z., Cao S., Zhang S., Biesiada M., Wu Y., Zhu Z.-H., 2019, MNRAS, 483, 1104
Ratra B., Peebles P. J. E., 1988, Phys. Rev. D, 37, 3406

Rezaei M., Ojaghi S. P., Malekjani M., 2020, ApJ, 900, 70
Riess A. G. et al., 1998, AJ, 116, 1009
Risaliti G., Lusso E., 2015, ApJ, 815, 33
Risaliti G., Lusso E., 2017, Astron. Nachr., 338, 329
Risaliti G., Lusso E., 2019, Nat. Astron., 3, 272
Ryan J., Chen Y., Ratra B., 2019, MNRAS, 488, 3844
Schwarz G., 1978, Ann. Stat., 6, 461
Scolnic D. M. et al., 2018, ApJ, 859, 101
Shi K., Huang Y. F., Lu T., 2012, MNRAS, 426, 2452
Siegel E. R., Guzmán R., Gallego J. P., Orduña López M., Rodríguez Hidalgo P., 2005, MNRAS, 356, 1117
Sollerman J. et al., 2009, ApJ, 703, 1374
Sotiriou T. P., Faraoni V., 2010, Rev. Mod. Phys., 82, 451
Spergel D. N. et al., 2003, ApJS, 148, 175
Suzuki N. et al., 2012, ApJ, 746, 85
Tegmark M. et al., 2004, Phys. Rev. D, 69, 103501
Terlevich R., Terlevich E., Melnick J., Chávez R., Plionis M., Bresolin F., Basilakos S., 2015, MNRAS, 451, 3001
Tsujikawa S., 2010, in Wolschin G., ed., Lecture Notes in Physics Vol. 800, Lectures on Cosmology: Accelerated Expansion of the Universe. Springer-Verlag, Berlin, p. 99
Virtanen P.et al., 2020, Nat Methods, 17, 261
Vishwakarma R. G., 2001, Classical Quantum Gravity, 18, 1159
Wang Y., Freese K., Gondolo P., Lewis M., 2003, ApJ, 594, 25
Wang J.-M., Du P., Valls-Gabaud D., Hu C., Netzer H., 2013, Phys. Rev. Lett., 110, 081301
Watson D., Denney K. D., Vestergaard M., Davis T. M., 2011, ApJ, 740, L49
Wei J.-J., Wu X.-F., Melia F., 2016, MNRAS, 463, 1144
Weinberg S., 1989, Rev. Mod. Phys., 61, 1
Wu Y., Cao S., Zhang J., Liu T., Liu Y., Geng S., Lian Y., 2020, ApJ, 888, 113
Xia J.-Q., 2009, Phys. Rev. D, 79, 103527
Xu T., Cao S., Qi J., Biesiada M., Zheng X., Zhu Z.-H., 2018, J. Cosmol. Astropart. Phys., 06, 042
Yang R.-J., 2011, Eur. Phys. J. C, 71, 1797
Yang T., Banerjee A., Ó Colgáin E., 2020, Phys. Rev. D, 102, 123532
Zheng X., Ding X., Biesiada M., Cao S., Zhu Z.-H., 2016, ApJ, 825, 17
Zheng X., Biesiada M., Cao S., Qi J., Zhu Z.-H., 2017, J. Cosmol. Astropart. Phys., 10, 030
Zheng X., Liao K., Biesiada M., Cao S., Liu T.-H., Zhu Z.-H., 2020, ApJ, 892, 103
Zheng X.-G., Cao S., Biesiada M., Li X.-L., Liu T.-H, Liu Y.-T., 2021, Sci. China Phys., Mech. Astron., 64, 259511
Zhu Z.-H., Fujimoto M.-K., 2002, ApJ, 581, 1
Zlatev I., Wang L., Steinhardt P. J., 1999, Phys. Rev. Lett., 82, 896

This paper has been typeset from a TEX/LATEX file prepared by the author.